

Article

Applying a Series and Parallel Model and a Bayesian Networks Model to Produce Disaster Chain Susceptibility Maps in the Changbai Mountain area, China

Lina Han ^{1,2}, Jiquan Zhang ^{1,3,*} , Yichen Zhang ⁴ and Qiuling Lang ⁵

¹ School of Environment, Northeast Normal University, Changchun 130024, China; hanln301@nenu.edu.cn

² Key Laboratory for Vegetation Ecology, Ministry of Education, Changchun 130117, China

³ State Environmental Protection Key Laboratory of Wetland Ecology and Vegetation Restoration, Northeast Normal University, Changchun 130117, China

⁴ Jilin Institute of Geological Environment Monitoring, Changchun 130061, China; weifenfangcheng@tom.com

⁵ Changchun Institute of Technology, Changchun 130021, China; 0215046@ccit.edu.cn

* Correspondence: zhangjq022@nenu.edu.cn; Tel.: +13596086467

Received: 9 September 2019; Accepted: 14 October 2019; Published: 15 October 2019



Abstract: The aim of this project was to produce an earthquake–landslide debris flow disaster chain susceptibility map for the Changbai Mountain region, China, by applying data-driven model series and parallel model and Bayesian Networks model. The accuracy of these two models was then compared. Parameters related to the occurrence of landslide and debris flow disasters, including earthquake intensity, rainfall, elevation, slope, slope aspect, lithology, distance to rivers, distance to faults, land use, and the normalized difference vegetation index (NDVI), were chosen and applied in these two models. Disaster chain susceptibility zones created using the two models were then contrasted and verified using the occurrence of past disasters obtained from remote sensing interpretations and field investigations. Both disaster chain susceptibility maps showed that the high susceptibility zones are situated within a 10 km radius around the Tianchi volcano, whereas the northern and southwestern sections of the study area comprise primarily very low or low susceptibility zones. The two models produced similar and compatible results as indicated by the outcomes of basic linear correlation and cross-correlation analyses. The verification results of the ROC curves were found to be 0.7727 and 0.8062 for the series and parallel model and BN model, respectively. These results indicate that the two models can be used as a preliminary base for further research activities aimed at providing hazard management tools, forecasting services, and early warning systems.

Keywords: landslide; debris flow; series and parallel model; Bayesian Networks model; susceptibility; Changbai Mountain

1. Introduction

In some countries of the world, earthquakes may constitute catastrophic natural disasters. Each earthquake may induce diverse secondary disasters and cause many deaths and injuries. In 2008, a catastrophic earthquake with Ms (surface wave magnitude) 7.9 occurred in Sichuan, China, triggering 197,481 landslides and leading to a total of 69,225 fatalities with an additional 17,393 people counted as missing [1,2]. On February 27, 2010, a disastrous earthquake with Ms 8.8 occurred in a coastal region of central Chile, resulting in 525 fatalities and approximately 20 billion dollars in economic losses, and is estimated to have influenced the lives of over 8 million people [3,4]. On March 11, 2011, an earthquake with Ms 9.0 occurred in the Tohoku region of Japan, triggering a large tsunami that

severely damaged infrastructure—such as traffic and energy supply systems—and caused more than 19,000 fatalities and 200–300 billion dollars in economic losses [5,6]. The phenomenon whereby a series of secondary disasters are induced by some primary disaster is termed a disaster chain [7,8]. In 2002, Shi [9] described typhoon-rainstorm disaster chains, cold wave disaster chains, dry disaster chains, and earthquake disaster chains based on diverse disaster chain types. Guo [10] classified disaster chains into causal chains, homologous chains, mutually exclusive chains, and row chains based on disaster chain space-time structure. The damages and losses caused by disaster chains are believed to often be much greater than those caused by the individual disasters themselves [11,12]. Disaster chain susceptibility assessment has, therefore, become increasingly important and urgent.

The susceptibility evaluation of disaster chains is indispensable for efficient urban development projects and emergency preparedness and response. Therefore, identified susceptibility zones ought to become a fundamental tool for making correlative decisions. Thus, it is important to elaborate on new methods to identify the susceptibility zones of at-risk regions and to guide decision-makers responsible for prevention and reduction strategies. Disaster chain susceptibility maps indicate that areas, where successive disasters are likely to take place in the future, are related using certain parameters of disasters that have occurred in the past. Many diverse methods, mainly statistical and deterministic, have been used to produce landslide susceptibility maps induced by earthquakes or rainfall [13]. The statistical methods typically assess the relationship between landslides and their related parameters and then predict landslide susceptibility zones [14]. For example, Regmi [15] applied a bivariate statistical model to map landslide susceptibility in regions affected by earthquakes. The statistical probabilistic likelihood-frequency ratio (PLFR) model and an artificial neural network (ANN) model were used to obtain earthquake- or heavy rainfall-induced landslide susceptibility zones in Dou [16]. Shrestha [17] applied logistic regression (LR) and analysis of covariance (ANCOVA) models to evaluate earthquake-induced landslide susceptibility. Cao [18] assessed seismic landslide susceptibility based on LR and random forest (RF) models and contrasted their assessment accuracy. In the work of Bathrellos [19,20], landslide, flood, and seismic hazard assessment maps were generated separately, combined with an analytical hierarchy process (AHP), and used to produce a multi-hazard map with a geographical information system (GIS). Chousianitis [21] used a parametric time probabilistic approach to evaluate earthquake-induced landslide hazards in Greece. Hakan [22] developed an improved global statistical method to predict the landslides induced by earthquakes in near real-time. Sansar [23] applied GIS-based statistical models to map landslide susceptibility zones at a regional level.

Deterministic methods can offer quantitative data on disasters and can be used immediately for engineering design and risk identification. Both these methods require sufficient detailed data on the basis of laboratory tests or field measurements, and therefore can only be used for small regions. Melo [24] used a dynamic model to simulate debris flow run-out. Oliveira [25] assessed shallow slide susceptibility at the basin scale based on a combination of statistical and physical methods. Byron [26] applied a dynamic landslide run-out model (ASCHFLOW) to analyze medium-scale hazards. Huang [27] calculated the possible landslides induced by earthquakes under different ground shaking scenarios. Salinas-Jasso [28] evaluated regional seismic landslide hazards by calculating coseismal displacements in terms of damage related to regional slope failures. Chen [29] applied the Newmark method of rigid-block modeling to evaluate the distribution of earthquake-triggered landslides.

In physics, a series circuit is a circuit comprising elements connected one by one in sequence, whereas a parallel circuit is a circuit comprising elements connected side by side. Zhang [30] applied series and parallel structures in a cooler network in order to reduce energy consumption and enhance economic benefit. A primary-parallel-secondary-series (PPSS) structure was proposed to realize output-voltage sharing ability for HV (high-voltage) generator applications [31]. Cheng [32] adopted the series-parallel-series compensation method to acquire self-governed power control of the total loads for each repeater unit. Tian [33] used the series and parallel model to evaluate the hazard of landslides on the basis of disaster conditions and applications.

The Bayesian networks (BN) model is expressed as a graphical network representing causal relationships between diverse nodes. BN models have been successfully applied in many areas, for example, medical sciences, image processing, artificial intelligence, and environmental and ecological sciences [34]. Factors influencing medicine use behavior in adolescents in Japan were also analyzed using Bayesian Networks [35]. Lee [36] applied Markov chain Monte Carlo techniques and Bayesian inference to develop efficient and tractable spatial loss field (SLF), estimators. Bayesian artificial intelligence analyses were also used to reveal non-obvious correlations for disease management with data from the United States Centers for Medicare and Medicaid Services (US CMS) [37]. Trifonova [38] applied a dynamic BN model to predict ecosystem components and their responses to climate variability.

Based on the above studies, this study aims to apply the data-driven model (series and parallel model and Bayesian Networks model) to evaluate and compare earthquake-landslide-debris flow disaster chain susceptibility zones in the Changbai Mountain area, China. We note that the series and parallel model has not been used to assess the susceptibility of disaster chains in the field of natural disasters. In addition, the accuracy of the Bayesian Networks model has not been verified and validated. In this study, we therefore assess the earthquake-landslide-debris flow disaster chain susceptibility by utilizing both the series and parallel model and the Bayesian Networks model, and compare the accuracy of these two methods, the former of which has not previously been used for this application and the latter of which is the one typically used in previous studies. These two susceptibility assessment models and case studies may offer a framework and tools for seismic disaster chain susceptibility identification and evaluation.

2. Methodologies

The main aim of this research is to apply the data-driven model (series and parallel model and the BN model) to evaluate the earthquake-landslide-debris flow disaster chain susceptibility in the Changbai Mountain area, China. Detailed disaster inventories were obtained from the visual interpretation of remote sensing data prepared by the Jilin Institute of Geological Environment Monitoring (JIGEM). All disaster points (defined as the locations of past disaster events) were randomly selected and divided into two groups for training and verification. A portion of the disaster points with correlatively calculated or extracted parameters was used for the series and parallel and BN models to obtain the disaster chain susceptibility map. The remaining disaster points were applied for comparison and verification purposes. According to Fabbri [39], the classification of disaster positions for a precise verification process is significant. Based on this objective, three classification methods—time of disaster occurrence, space of disaster occurrence, and random classification—were proposed [40]. Among these, space and random classification were applied together for 360 disaster points (that is, the location of the occurrence of a past disaster) that occurred in Jilin province as the exact occurrence time of these disaster incidents is not known precisely. The 360 disaster points were selected for initiation locations, 200 disaster points were landslide, 160 disaster points were debris flow, and landslide and debris flow were triggered by the earthquake and rainfall. These disaster points were divided into two portions: those that occurred in the Changbai Mountain region and those that occurred in other regions. Ninety disaster points occurred in the Changbai Mountain region. The 210 disaster points observed in other areas of Jilin province were used for calibration, and the remaining 60 points were used to validate the series and parallel and BN models. Basic linear correlation and cross-correlation methods were then applied to compare the models. Finally, relative operating characteristics (ROC) curves were used to validate the accuracy of the susceptibility results obtained from the models. Figure 1 illustrates the described methodology.

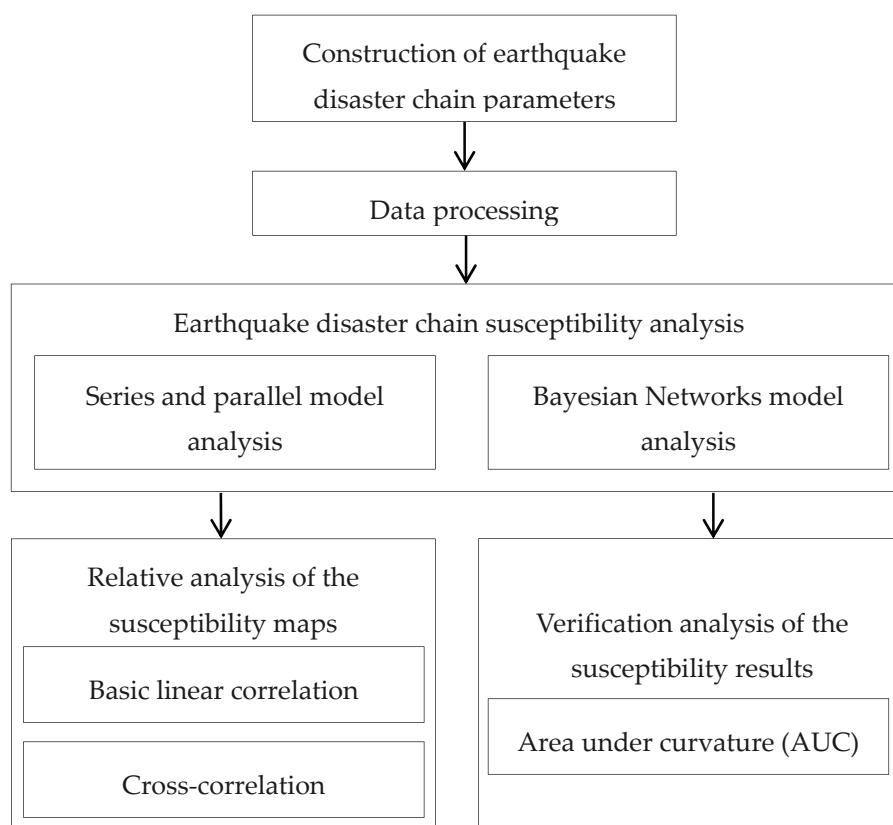


Figure 1. Flowchart showing the methodology employed in this study.

2.1. Study Area

The Changbai Mountain region comprises a total area of approximately 3278 km² and is situated in Jilin Province, China (Figure 2). In the study area, the terrain is generally high in the center, low in northeast, northwest, and southwest, with a stepped topography descending to the south and southwest. Mountains and hills also exist in the area with v-shaped gullies producing significant relief. The rock types in the area consist mainly of basalt, granite, alkali trachyte, and trachyte breccia, with the basaltic rocks accounting for three-quarters of the surface area. The study area belongs to the North Temperate Zone with a continental monsoon climate. The climate is characterized by four seasons with long, cold winters and short, wetter summers. The average temperature is 2.1–3.3°C, the extreme minimum temperature is 36.4°C, and the extreme maximum temperature is 40.5°C. The average rainfall is 632–1407.6 mm, with about 60% of annual rainfall. Large and concentrated rainfall events have created favorable conditions for triggering landslides.

Tianchi volcano is a well-known volcano located in the area, capable of potentially catastrophic eruptions. According to monitoring data, the volcanic activity has shown a clearly increasing trend since 2000, and therefore the possibility of an eruption has also increased. More than 200 earthquakes with magnitudes greater than 1 have occurred each year. The topography and geomorphology of the study area are very complex and there are numerous large mountains and rivers distributed throughout the region. As a result, geological disasters have occurred with a high frequency. According to the monitoring data available in the Changbai Mountain region, landslides and debris flow typically occur during and after earthquakes or heavy rainfall. The minimum affected area by such landslides in the dataset is around 120 m² and the maximum is 324,000 m². If the volcano erupts in the future, associated earthquakes and other geological processes may result in a disaster chain. Based on the locations, types and other features such as degree of damage and occurrence frequency of past events, the earthquake-landslide-debris flow disaster chain was selected as the focus of this study.

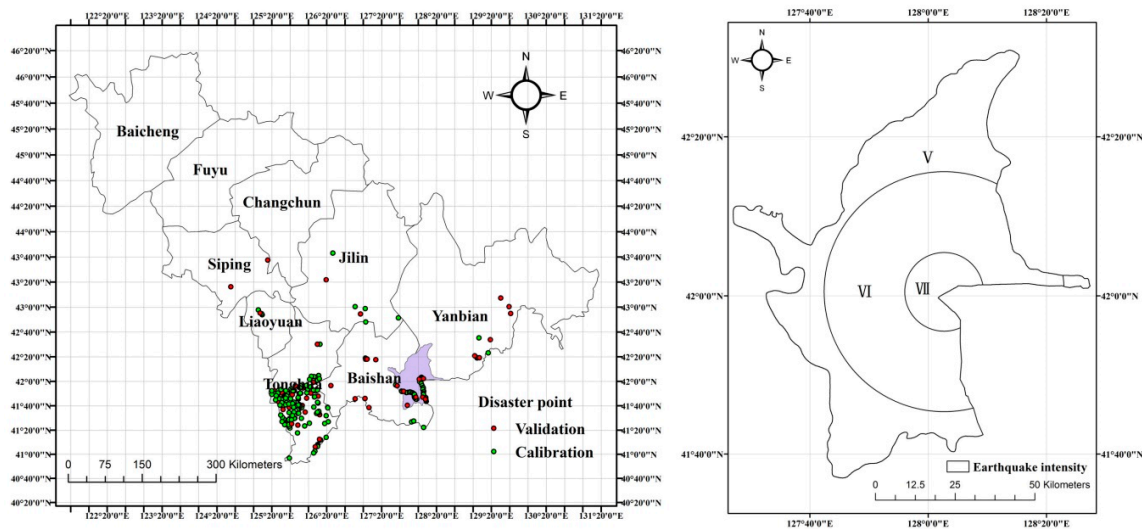


Figure 2. The map of disaster points' location, and earthquake intensity zones of the study area.

2.2. Series and Parallel Model

2.2.1. Circuit Principle

Figure 3 shows the basic series and parallel circuit structure in physics. R_1 , R_2 , and R_3 represent the resistance values of three electrical appliances. S represents a closed switch. R_2 and R_3 form a parallel circuit and R_1 forms a series circuit again. When S is closed, the circuit is connected, there is current in the circuit and it is in the path state, the resistance and current in the circuit can be calculated using formulas (1)–(3):

$$R = R_1 + R_{23} \tag{1}$$

$$R_{23} = \frac{1}{\frac{1}{R_2} + \frac{1}{R_3}} \tag{2}$$

$$I = \frac{U}{R} \tag{3}$$

where R is the total resistance in the circuit, R_1 , R_2 , R_3 are the resistance values of the electrical appliances, R_{23} is the parallel circuit resistance, U is the voltage in the circuit, and I is the electric current in the circuit.

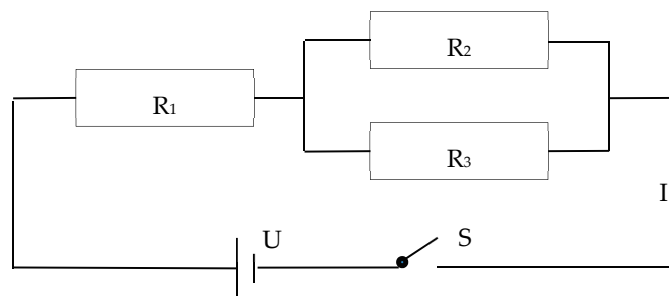


Figure 3. Map of the structure of a series and parallel circuit.

2.2.2. Analysis of Disaster Development Conditions

The development conditions for disasters can be classified into two groups: the internal development conditions and external trigger conditions. The former include the geological and geomorphological conditions that constitute the internal causes and are essential to the occurrence of every disaster event. The latter include the external factors that act on a slope, acting on the internal

conditions to push them to play a role in the event, intensifying the contradiction between sliding and anti-sliding, and thus accelerating the slope to slide. One or several external trigger factors can stimulate the internal development conditions to play a part in the occurrence of disaster events.

Following the above analysis, the development mechanism for disaster events can be analogized to the series-parallel circuit principle. In this study, three elements of the circuit were applied to define the occurrence mechanism of disaster events. The regional background condition of disaster development is defined as the voltage U . The trigger parameters and internal parameters are defined as the total resistance R in the circuit and represent the capacity to prevent the disaster from occurring. The current is defined as the degree of disaster susceptibility under the regional background conditions and the various parameter conditions that work together to prevent disaster occurrence. In terms of the disaster development mechanism, parameters corresponding to earthquake intensity (the extent of earthquake impact and damage) and mean annual rainfall are classified as trigger factors, whereas the elevation, slope, slope aspect, lithology, distance to rivers and distance to faults are categorized as internal development factors for landslide occurrence [41–43]. For debris flow occurrence, the parameters corresponding to landslide occurrence, earthquake intensity, and mean annual rainfall are classified as trigger factors whereas elevation, slope, slope aspect, lithology, distance to rivers, distance to faults, land use, and the normalized difference vegetation index (NDVI) are classified as internal development factors [44,45].

2.2.3. Evaluation of the Series and Parallel Model of Disaster Chain Susceptibility

According to the development conditions for disaster and the series and parallel circuit principle, the internal parameter and trigger parameter systems constitute first-order series circuits and the internal parameter and trigger parameter systems are each composed of one or more parallel circuits. The earthquake-landslide-debris flow disaster chain susceptibility can, therefore, be calculated using the following equation:

$$I = \frac{U}{R(\text{total})} \quad (4)$$

$$R(\text{total}) = R(\text{trigger}) + R(\text{internal}) \quad (5)$$

$$R(\text{trigger}) = \frac{1}{\sum_{i=1}^n \frac{1}{R_i}} \quad (i = 1, 2, \dots, n) \quad (6)$$

$$R(\text{internal}) = \frac{1}{\sum_{j=1}^n \frac{1}{R_j}} \quad (j = 1, 2, \dots, n) \quad (7)$$

where $R(\text{trigger})$ and $R(\text{internal})$ are the resistance values of the trigger and internal parameter systems, respectively, and R_i and R_j are the resistance values of every parameter in the system.

As the study region is small and we only focus on one area, the regional background condition, the voltage U , is defined as a fixed value of 1 V. The combined action of trigger factors and internal factors to prevent disaster occurrence is R . In this paper, R is assumed to be 1 and the resistance of the trigger and internal parameter systems are each thought to be 0.5. The importance of all related factors for the disaster events was determined based on previous studies of landslides and debris flows [46–53]. Where the importance was greater, the resistance value was smaller. The Golden Section method was used to assign the resistance values of the different factors. Different categories of each factor in the parameter system were determined according to formulas (6)–(7) and the results are listed in Tables S1 and S2.

2.3. Bayesian Networks Model

2.3.1. Bayesian Networks Principle

Bayesian Networks (BN) are powerful modeling tools that replicate the essential features to ratiocinate uncertainty in a consistent, efficient and sound mathematic way [54]. In BN models, the network structure is a directed acyclic graph (DAG) that graphically represents the logical relationship between nodes, and the network parameter is the conditional probability that quantifies the strength of this relationship [55–57]. The network structure and network parameter can be acquired through professional opinion or knowledge inspiration [58,59] or training from data [60,61]. Figure 4 shows a sample BN model, in which the node L is a parent node of the child nodes M and N, and node M is a parent node of the child node N. The arrows between the two nodes represent edges. The joint probability of Bayesian networks can be expressed as the product of the edge probability of each node:

$$P(L, M, N) = P(L) \times P(M|L) \times P(N|L, M) \quad (8)$$

where $P(L)$ is the prior probability that is the conditional probability without parent nodes, $P(M|L)$ is the conditional probability that is the occurrence probability of M under the L conditions, $P(N|L, M)$ is the conditional probability that is the occurrence probability of N under the L and M conditions.

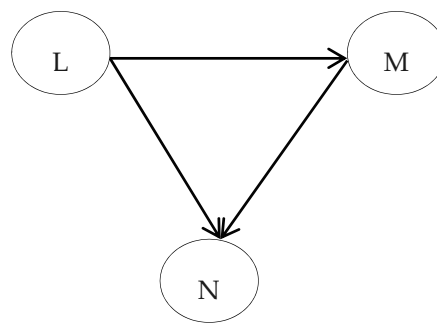


Figure 4. A simple Bayesian Network structure.

2.3.2. Bayesian Network Model Construction for the Earthquake Disaster Chain

The disaster itself is defined as a variation in the Earth's surface system, comprising the disaster environment, hazard factor, and disaster body. Thus, the disaster is the outcome of the coaction of the elements in the system [62]. According to a system theory viewpoint, earthquake, landslide and debris flow events are considered as a system. Various factors related to the three disaster events can be considered network nodes that affect the state of the disaster event and promote disaster event occurrence, describe the nature and characteristics of an earthquake disaster chain system, and can be used to assess the disaster chain susceptibility [63]. In this paper, in accordance with the conditional parameters and causal relationship between the near-disaster events, the earthquake intensity, mean annual rainfall, elevation, slope, slope aspect, lithology, distance to rivers, distance to faults, land use and NDVI were chosen as network nodes in the BN model. The Bayesian Network structure of an earthquake-landslide-debris flow disaster chain is shown in Figure 5. The network parameter of the earthquake disaster chain was determined using the Gradient technique in the software Netica.

All parameters (earthquake intensity, mean annual rainfall, elevation, slope, slope aspect, lithology, distance to rivers, distance to faults, land use, and NDVI) related to earthquake-induced secondary disasters are shown in Figure 6. The earthquake intensity was determined using the intensity attenuation formula for eastern China [64–66] and is shown in Figure 2. A 30 m × 30 m digital elevation model was extracted from 1:50,000 topographical maps prepared by JIGEM and used to obtain elevation, slope and slope aspect parameters. The lithology map was digitized from 1:200,000 geologic maps. To establish the distance to rivers and the distance to faults, drainage lines, and fault lines were digitized from a drainage line distribution dataset and a fault line distribution dataset at a 1:250,000 scale. The land use map was obtained from a land-use dataset. The NDVI map was extracted from Landsat satellite imagery. The mean annual rainfall map was provided by JIGEM.

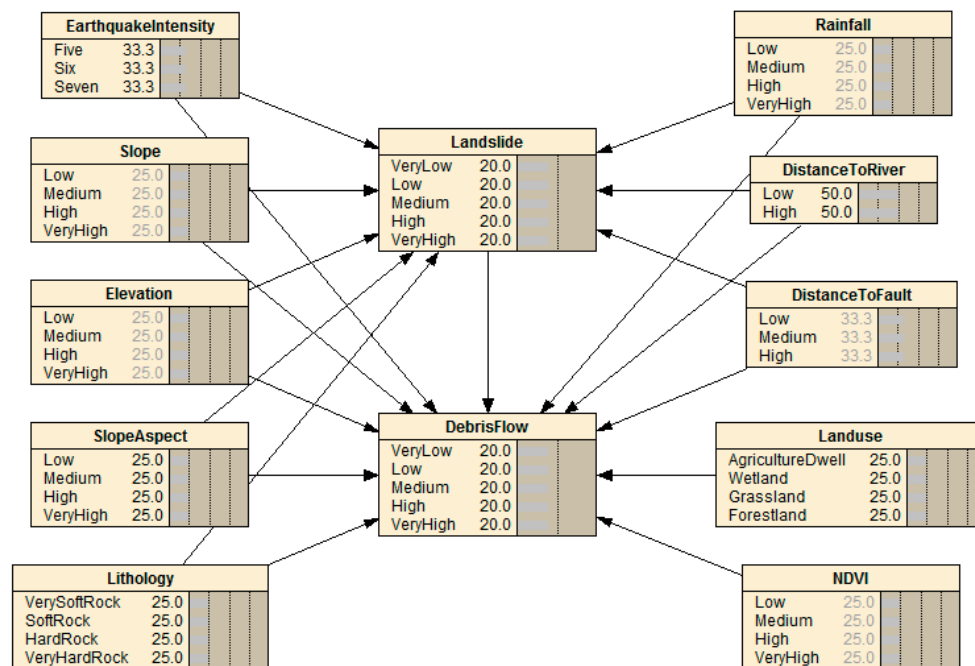


Figure 5. The Bayesian Networks model structure for an earthquake disaster chain.

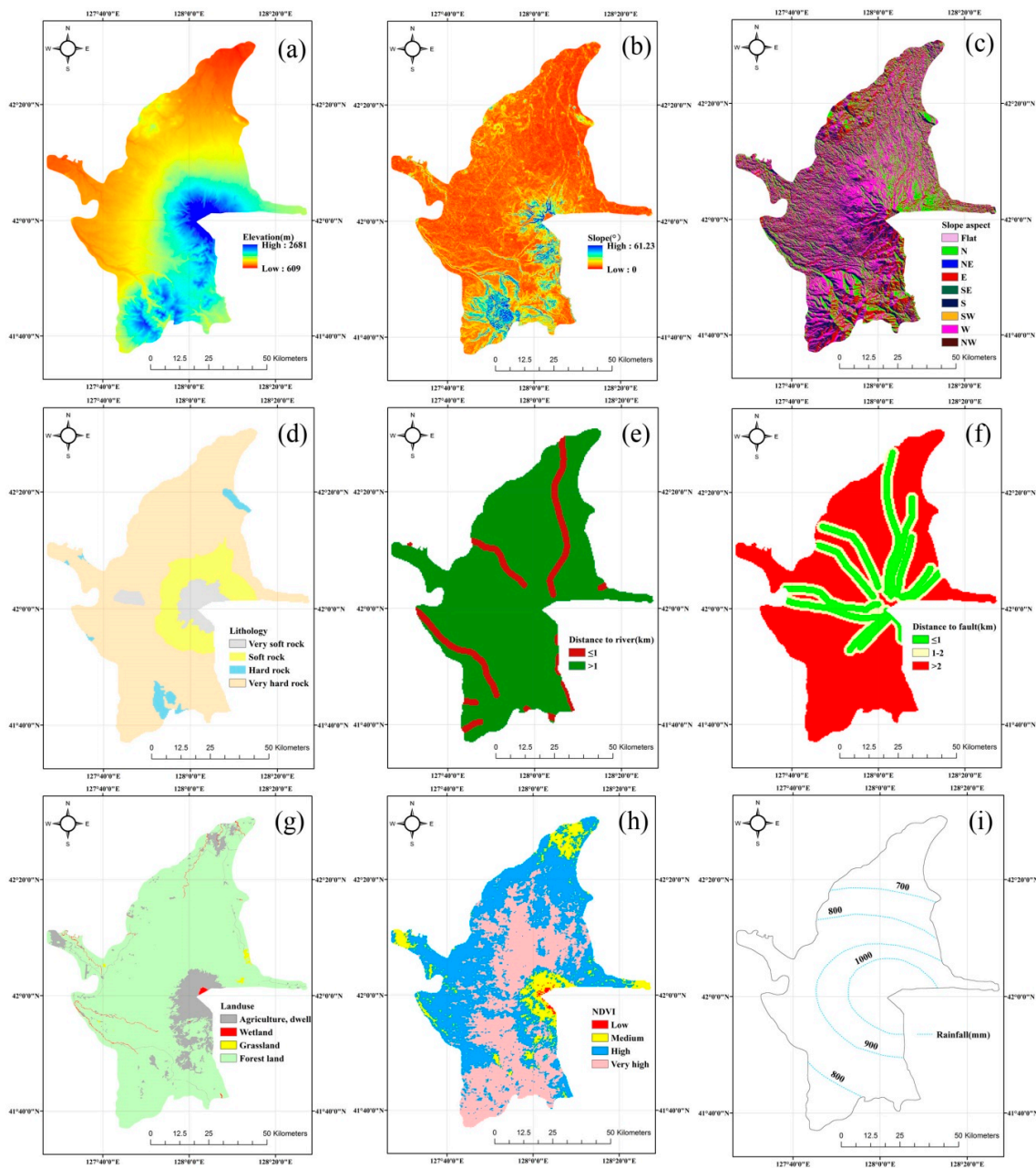


Figure 6. Condition parameters: (a) Elevation, (b) Slope, (c) Slope aspect, (d) Lithology, (e) Distance to river, (f) Distance to fault, (g) Land use, (h) NDVI, (i) Rainfall.

3. Results

3.1. Disaster Chain Susceptibility Assessment from the Series and Parallel Model

The earthquake-landslide and earthquake-landslide-debris flow disaster chain susceptibility maps obtained from the series and parallel model are shown in Figure 7a,b, respectively. They are shown with five susceptibility levels to enhance readability. The susceptibility zones obtained for these two disaster chains are clearly similar, with the northern and southeastern sections of the study area primarily consisting of very low to low susceptibility zones, whereas the very high and high susceptibility zones are situated predominantly within a 10 km radius of the Tianchi volcano. On the earthquake-landslide disaster chain susceptibility map, a total of 39.63% of the area is characterized by very low susceptibility. Low, medium, and high susceptibility areas make up 34.03%, 13.27%, and 8.65%

of the total area, respectively. The very high susceptibility zones make up 4.42% of the total studied area. For the earthquake–landslide–debris flow disaster chain susceptibility map, a total of 43.74% of the study area is characterized by very low susceptibility. Low, medium, and high susceptibility areas account for 32.54%, 11.45%, and 6.4% of the total area, respectively. The very high susceptibility zones make up 5.88% of the area.

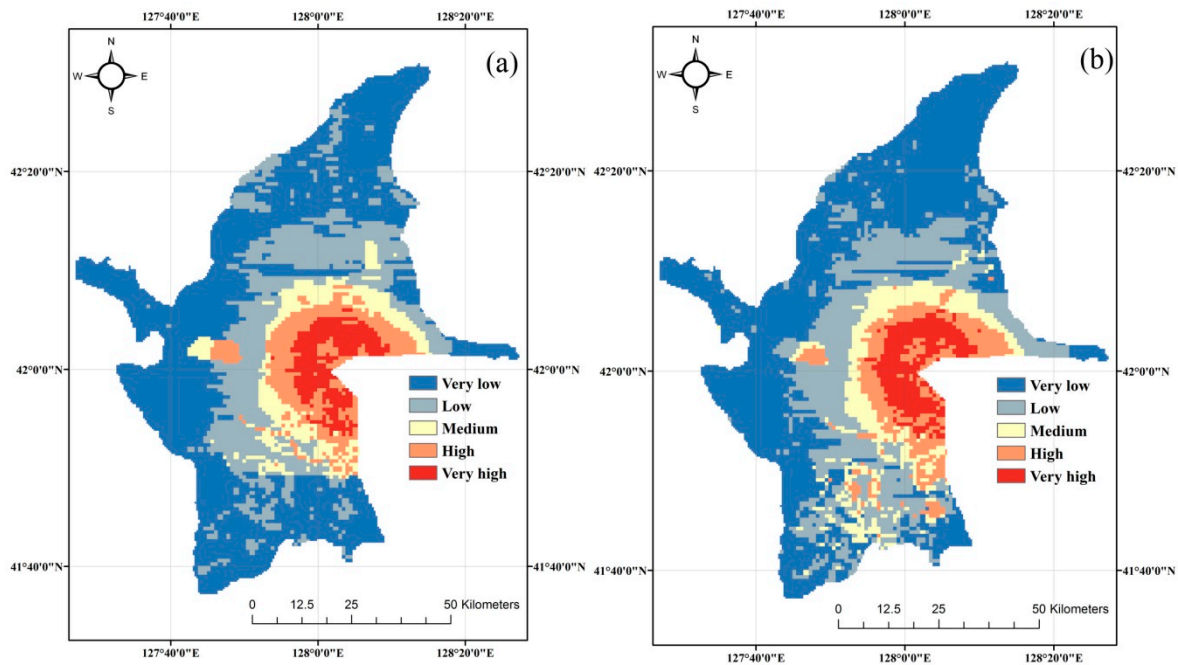


Figure 7. Series and parallel model disaster chain susceptibility maps for the chains: (a) Earthquake-landslide, and (b) Earthquake-landslide-debris flow.

3.2. Disaster Chain Susceptibility Assessment of Bayesian Networks Model

The studied area was segmented into $1 \text{ km} \times 1 \text{ km}$ grid cells, resulting in 5922 grid cells. The choice of a cell with a resolution of 1 km^2 is due to software limitations and this is a drawback that needs to be addressed in future research. The attributed values (earthquake intensity, precipitation, elevation, slope, slope aspect, lithology, distance to rivers, distance to faults, land use and NDVI) for each cell center point were extracted using spatial analysis tools in ArcGIS software. The grid cell data were then converted into case file format and input into the BN model in the Netica software, and the probabilities of the earthquake-landslide and earthquake-landslide-debris flow disaster chains were obtained from the BN model. The susceptibility maps of the earthquake-landslide and the earthquake-landslide-debris flow disaster chains are shown in Figure 8a,b, respectively. The susceptibility zones from the BN model are broadly similar to those from the series and parallel model. According to the two maps, 52.9%, 24.45%, 8.38%, 8.81%, and 5.45% of the studied area is characterized by very low, low, medium, high, and very high susceptibility to an earthquake-landslide disaster chain, respectively. In the same way, 49.51%, 26.04%, 9.84%, 8.76% and 5.84% of the studied area are characterized by very low, low, medium, high, and very high susceptibility to an earthquake-landslide-debris flow disaster chain, respectively.

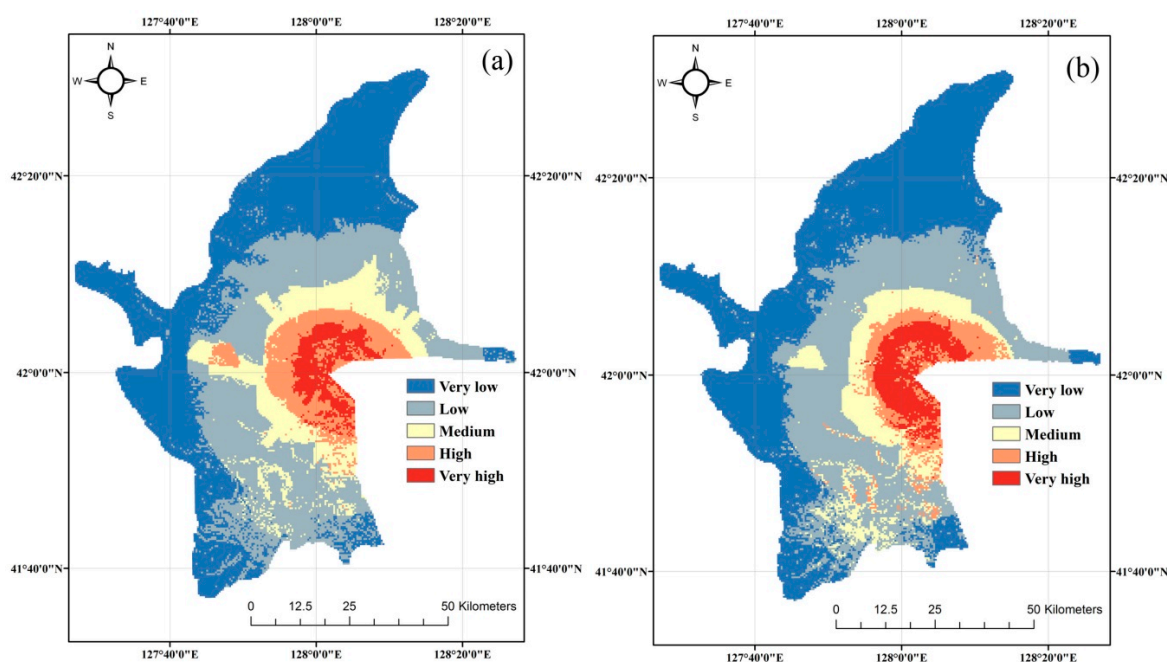


Figure 8. BN model disaster chain susceptibility maps for the chains: (a) Earthquake-landslide and (b) Earthquake-landslide-debris flow.

3.3. Relative Analysis of the Susceptibility Evaluation Results

The four susceptibility maps (the two earthquake-landslide disaster chain susceptibility maps and the two earthquake-landslide-debris flow disaster chain susceptibility maps) obtained from the series and parallel model and the Bayesian Networks model were contrasted by applying basic linear correlation and cross-correlation methods, and the results are shown in Table 1. The coefficients between the series and the parallel model and Bayesian Networks model were found to be 0.8267 for the earthquake-landslide disaster chain and 0.9384 for the earthquake-landslide-debris flow disaster chain.

The cross-correlation method included two-ways named image cross-tabulation and a calculation of the kappa index value (KIA). The image cross-tabulation can be obtained by measures such as Cramer's V, a relative coefficient ranging between 0 and 1, which indicates an uncorrelated relationship and a perfect correlation, respectively [67]. In addition, the importance of Cramer's V should also be determined by obtaining a chi-square value. The relative coefficient of Cramer's V between the series and parallel model and Bayesian Networks model is 0.71 for the earthquake-landslide disaster chain and 0.782 for the earthquake-landslide-debris flow disaster chain, and the corresponding chi-square values are 11941.334 and 14497.015, respectively. The cross-correlation measure was taken as the kappa index value, which is an index ranging between 0 and 1. When the classifications in these two maps describe an identical type data with identical data categories, the kappa index value has meaning [68]. The value can, therefore, express the comparability between the calculated susceptibility zones. The kappa index value is 0.602 for the earthquake-landslide disaster chain and 0.757 for the earthquake-landslide-debris flow disaster chain.

Table 1. The relative analysis results between the series and parallel model and the Bayesian Networks model.

	Earthquake-landslide	Earthquake-landslide-debris flow
Correlation coefficients	0.8267	0.9384
Cramer's V	0.71	0.782
Chi-square	11941.334	14497.015
Kappa index	0.602	0.757

3.4. Verification of the Different Susceptibility Evaluation Models

To confirm the precision of the two disaster chain susceptibility maps obtained from the series and parallel model and the Bayesian Networks model, the relative operating characteristics (ROC) method was applied. According to the ROC method, the validation of the two models is achieved by correctly estimating the occurrence or non-occurrence of disaster chains in accordance with the training and verification dataset. The ROC curves for the earthquake-landslide-debris flow disaster chain susceptibility assessment are shown in Figure 9a,b. The area under the ROC curve (AUC) method was applied to express the precision of the evaluation model, and the values may range between 0.5 and 1.0, indicating inaccurate evaluation and perfect evaluation, respectively [69]. The AUC values of the susceptibility evaluation results obtained from the series and parallel model and the Bayesian Networks model were found to be 0.7727 and 0.8062, respectively.

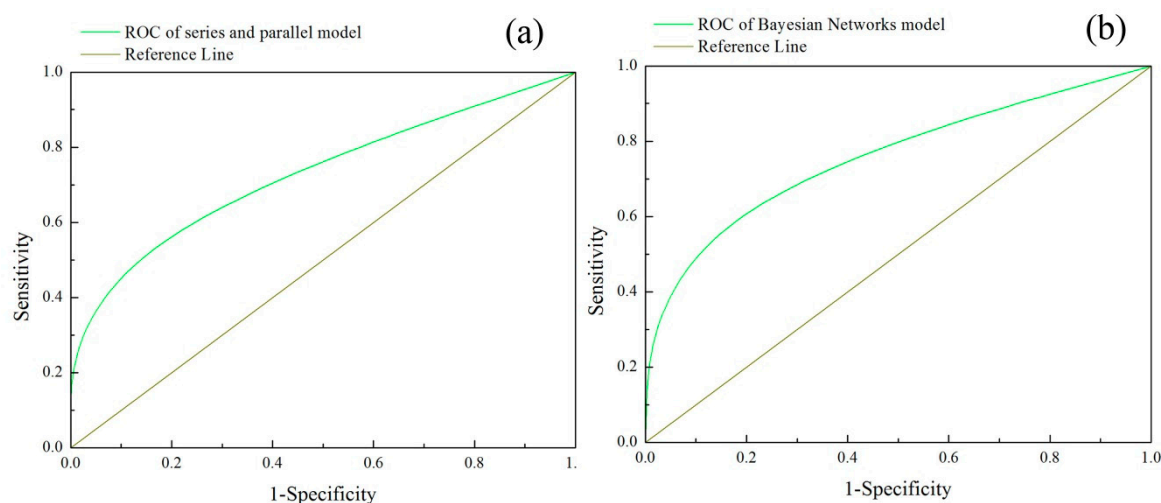


Figure 9. The ROC curve of the susceptibility assessment results for (a) The series and parallel model, (b) The Bayesian Networks model.

4. Discussions

A series and parallel model and a Bayesian Networks model were applied to produce susceptibility zones for the occurrence of earthquake-landslide-debris flow disaster chains in the Changbai Mountain area, using ten correlative parameters. The quantitative susceptibility evaluation of the earthquake disaster chain was successfully achieved. The earthquake-landslide and earthquake-landslide-debris flow disaster chain susceptibility maps obtained from the two models were similar. The susceptibility zone results show that the northern and southeast sections of the study area primarily comprise very low to low susceptibility zones, and the very high and high susceptibility zones are predominantly situated within a 10 km radius of the Tianchi volcano. In particular, the high susceptibility zones were characterized by high elevation and high slopes. The susceptibility zones were similar in terms of the precipitation and lithology contours. From this analysis, we can conclude that the susceptibility zones for the earthquake disaster chains were determined mainly by the parameters of elevation, slope, precipitation, and lithology. In addition to this, the very high susceptibility zone for the earthquake-landslide-debris flow disaster chain is higher than that for the earthquake-landslide disaster chain using both methods. The most likely reason for this result is that landslides contribute to the occurrence of debris flows due to the generation of an additional volume of loose deposits and the altered geological environment, such as exposed rock. As a result, primary landslide events can induce a change in the surrounding disaster environment, accelerating the occurrence of a secondary disaster and increasing the disaster chain susceptibility.

In order to assess the accuracy and similarity of the series and parallel and Bayesian Networks models, basic linear correlation and cross-correlation methods were applied in this study. The relative coefficients were found to be 0.8267 for the earthquake-landslide disaster chain and 0.9384 for the earthquake-landslide-debris flow disaster chain, therefore the earthquake-landslide-debris flow disaster chain susceptibility zones were found to be more consistent between the two models. In the same way, the image cross-tabulation and kappa index value in the cross-correlation methods showed the same trend, in that the earthquake-landslide-debris flow disaster chain susceptibility zones were more precise than the earthquake-landslide disaster chain susceptibility zones. The cross-correlation values showed that the similarity between the series and parallel and the Bayesian Networks models were apparent and compatible with the basic linear correlation. To confirm the precision of the two disaster chain susceptibility maps obtained from the two models, the relative operating characteristics (ROC) method was applied. In the ROC curve, the AUC values of the susceptibility evaluation results were found to be 0.7727 and 0.8062 for the series and parallel model and Bayesian Networks model, respectively. These results indicate that the two models can be used as a preliminary base for further research activities aimed at providing hazard management tools, forecasting services, and early warning systems.

5. Conclusions

Many catastrophic natural hazards such as volcanic eruptions and earthquakes can induce secondary disasters, multiplying the casualties and economic losses, therefore, disaster chain susceptibility assessment has become a critical and urgent research issue. The aim of this study was to apply data-driven methods (series and parallel model and Bayesian Networks model) to evaluate the earthquake-landslide-debris flow disaster chain susceptibility in the Changbai Mountain area, China, and to compare the accuracy of these two models. The main conclusions of this study are as follows:

- (1) Visual analysis of the four disaster chain susceptibility maps showed that the susceptibility zones obtained from the series and parallel model and the Bayesian Networks model are broadly similar. Very high and high susceptibility are predominantly located within a 10 km radius of the Tianchi volcano, whereas the northern and southwestern sections of the study area were identified as low and very low susceptibility zones.
- (2) The basic linear correlation and cross-correlation methods were applied to compare the series and parallel model and the Bayesian Networks model, and the correlation coefficients, Cramer's V and kappa index showed that the two models were similar and approximately compatible.
- (3) The verification results of the ROC curve for the two models were found to be 0.7727 and 0.8062 respectively, showing that two models have great potential for forecasting and early warning, and could be applied in emergency management for earthquake disaster chains in the future.

Supplementary Materials: The following are available online at <http://www.mdpi.com/2073-4441/11/10/2144/s1>, Table S1: The resistance values of different factors and different categories of each factor in landslide disaster according to Golden Section Method, Table S2: The resistance values of different factors and different categories of each factor in debris flow disaster according to Golden Section Method.

Author Contributions: Original idea and the study conception, L.H.; methodology design, Y.Z.; data collection and preprocessing Q.L.; Funding acquisition, J.Z.; manuscript draft, L.H.

Funding: This work was supported by: "13 Five-Year" Plan for Science & Technology Support (2018YFC1508804); The Key Scientific and Technology Research and Development Program of Jilin Province (20180201033SF); The Key Scientific and Technology Research and Development Program of Jilin Province (20180201035SF); The Key Scientific and Technology Program of Jilin Province (20170204035SF).

Acknowledgments: The authors are grateful to the anonymous reviewers for their insightful and helpful comments to improve the manuscript.

Conflicts of Interest: The authors declare no conflict of interest.

References

1. Zhao, X.Y.; Hu, K.; Burns, S.F.; Hu, H.T. Classification and sudden departure mechanism of high-speed landslides caused by the 2008 Wenchuan earthquake. *Environ. Earth Sci.* **2019**, *78*, 125. [[CrossRef](#)]
2. Qi, S.W.; Xu, Q.; Lan, H.X.; Zhang, B.; Liu, J.Y. Spatial distribution analysis of landslides triggered by 2008.5.12 Wenchuan Earthquake, China. *Eng. Geol.* **2010**, *116*, 95–108. [[CrossRef](#)]
3. Serey, A.; Pinero-Feliciangeli, L.; Sepulveda, S.A.; Poblete, F.; Petley, D.N.; Murphy, W. Landslides induced by the 2010 Chile megathrust earthquake: A comprehensive inventory and correlations with geological and seismic factors. *Landslides* **2019**, *16*, 1153–1165. [[CrossRef](#)]
4. Zhang, P.Z.; Restrepo, J.I.; Conte, J.P.; Ou, J.P. Nonlinear finite element modeling and response analysis of the collapsed Alto Rio building in the 2010 Chile Maule earthquake. *Struct. Des. Tall Spec. Build.* **2017**, *26*. [[CrossRef](#)]
5. Goda, K.; Pomonis, A.; Chian, S.C.; Offord, M.; Saito, K.; Sammonds, P.; Fraser, S.; Raby, A.; Macabuag, J. Ground motion characteristics and shaking damage of the 11th March 2011 Mw9.0 Great East Japan earthquake. *Bull. Earthq. Eng.* **2013**, *11*, 147–170. [[CrossRef](#)]
6. Lay, T. A review of the rupture characteristics of the 2011 Tohoku-oki Mw 9.1 earthquake. *Tectonophysics* **2018**, *733*, 4–36. [[CrossRef](#)]
7. Shi, P.J. Theory and practice of disaster study. *J. Nanjing Univ. (SI)* **1991**, *11*, 37–42.
8. Shi, P.J. Theory and practice of disaster study. *J. Nat. Disasters* **1996**, *5*, 8–19.
9. Shi, P.J. Theory on disaster science and disaster dynamics. *J. Nat. Disasters* **2002**, *11*, 1–9.
10. Guo, Z.J.; Qin, B.Y. Brief discussion on disaster physics. *J. Catastrophol.* **1987**, *2*, 25–33.
11. Bai, Y.; Zhang, J.S.; Wang, J.A. A Comparative Study of Snow Disasters in Northern and Southern China—Taking Freezing and Snow Disaster in 2008 and Snowstorm Disaster in 2009 as Examples. *J. Catastrophol.* **2011**, *26*, 14–19.
12. Chen, Y.; Hu, J.P.; Peng, F. Seismological challenges in earthquake hazard reductions: Reflections on the 2008 Wenchuan earthquake. *Sci. Bull.* **2018**, *63*, 1159–1166. [[CrossRef](#)]
13. Reichenbach, P.; Rossi, M.; Malamud, B.D.; Mihir, M.; Guzzetti, F. A review of statistically-based landslide susceptibility models. *Earth Sci. Rev.* **2018**, *180*, 60–91. [[CrossRef](#)]
14. Kargel, J.S.; Leonard, G.J.; Shugar, D.H.; Haritashya, U.K.; Bevington, A.; Fielding, E.J.; Fujita, K.; Geertsema, M.; Miles, E.S.; Steiner, J.; et al. Geomorphic and geologic controls of geohazards induced by Nepal's 2015 Gorkha earthquake. *Science* **2016**, *351*, aac8353. [[CrossRef](#)]
15. Regmi, A.D.; Dhital, M.R.; Zhang, J.Q.; Su, L.J.; Chen, X.Q. Landslide susceptibility assessment of the region affected by the 25 April 2015 Gorkha earthquake of Nepal. *J Mt. Sci.* **2016**, *13*, 1941–1957. [[CrossRef](#)]
16. Dou, J.; Yunus, A.P.; Tien Bui, D.; Sahana, M.; Chen, C.W.; Zhu, Z.F.; Wang, W.D.; Pham, B.T. Evaluating GIS-Based Multiple Statistical Models and Data Mining for Earthquake and Rainfall-Induced Landslide Susceptibility Using the LiDAR DEM. *Remote Sens.* **2019**, *11*, 638. [[CrossRef](#)]
17. Shrestha, S.; Kang, T.S. Assessment of seismically-induced landslide susceptibility after the 2015 Gorkha earthquake, Nepal. *Bull. Eng. Geol. Environ.* **2019**, *78*, 1829–1842. [[CrossRef](#)]
18. Cao, J.; Zhang, Z.; Wang, C.Z.; Liu, J.F.; Zhang, L.L. Susceptibility assessment of landslides triggered by earthquakes in the Western Sichuan Plateau. *Catena* **2019**, *175*, 63–76. [[CrossRef](#)]
19. Bathrellos, G.D.; Skilodimou, H.D.; Chousianitis, K.; Youssef, A.M.; Pradhan, B. Suitability estimation for urban development using multi-hazard assessment map. *Sci. Total Environ.* **2017**, *575*, 119–134. [[CrossRef](#)]
20. Skilodimou, H.D.; Bathrellos, G.D.; Chousianitis, K.; Youssef, A.M.; Pradhan, B. Multi-hazard assessment modeling via multi-criteria analysis and GIS: A case study. *Environ. Earth Sci.* **2019**, *78*, 47. [[CrossRef](#)]
21. Chousianitis, K.; Del Gaudio, V.; Sabatakakis, N.; Kavoura, K.; Drakatos, G.; Bathrellos, G.D.; Skilodimou, H.D. Assessment of Earthquake-Induced Landslide Hazard in Greece: From Arias Intensity to Spatial Distribution of Slope Resistance Demand. *Bull. Seismol. Soc. Amer.* **2016**, *106*, 174–188. [[CrossRef](#)]
22. Tanyas, H.; Rossi, M.; Alvioli, M.; van Westen, C.J.; Marchesini, I. A global slope unit-based method for the near real-time prediction of earthquake-induced landslides. *Geomorphology* **2019**, *327*, 126–146. [[CrossRef](#)]
23. Meena, S.R.; Ghorbanzadeh, O.; Blaschke, T. A Comparative Study of Statistics-Based Landslide Susceptibility Models: A Case Study of the Region Affected by the Gorkha Earthquake in Nepal. *ISPRS Int. Geo-Inf.* **2019**, *8*, 94. [[CrossRef](#)]

24. Melo, R.; van Asch, T.; Zezere, J.L. Debris flow run-out simulation and analysis using a dynamic model. *Nat. Hazards Earth Syst. Sci.* **2018**, *18*, 555–570. [[CrossRef](#)]
25. Oliveira, S.C.; Zezere, J.L.; Lajas, S.; Melo, R. Combination of statistical and physically based methods to assess shallow slide susceptibility at the basin scale. *Nat. Hazards Earth Syst. Sci.* **2018**, *17*, 1091–1109. [[CrossRef](#)]
26. Luna, B.Q.; Blahut, J.; van Asch, T.; van Westen, C.; Kappes, M. ASCHFLOW—A dynamic landslide run-out model for medium scale hazard analysis. *Geoenviron. Disasters* **2016**, *3*, 29. [[CrossRef](#)]
27. Huang, Y.; Zhao, L.Y.; Xiong, M.; Liu, C.; Lu, P. Critical slip surface and landslide volume of a soil slope under random earthquake ground motions. *Environ. Earth Sci.* **2018**, *77*, 787. [[CrossRef](#)]
28. Salinas-Jasso, J.A.; Ramos-Zuniga, L.G.; Montalvo-Arrieta, J.C. Regional landslide hazard assessment from seismically induced displacements in Monterrey Metropolitan area, Northeastern Mexico. *Bull. Eng. Geol. Environ.* **2019**, *78*, 1127–1141. [[CrossRef](#)]
29. Chen, X.L.; Liu, C.G.; Wang, M.M. A method for quick assessment of earthquake-triggered landslide hazards: A case study of the Mw6.1 2014 Ludian, China earthquake. *Bull. Eng. Geol. Environ.* **2019**, *78*, 2449–2458. [[CrossRef](#)]
30. Zhang, H.T.; Feng, X.; Wang, Y.F.; Zhang, Z. Optimization of Cooler Networks with Different Cooling Types in Series and Parallel Configuration. *Ind. Eng. Chem. Res.* **2019**, *58*, 6017–6025. [[CrossRef](#)]
31. Mao, S.J.; Chen, Y.; Li, C.M.; Li, W.H.; Popovic, J.; Ferreira, J.A. A Coupled-Inductor-Based LCC Resonant Converter with the Primary-Parallel-Secondary-Series Configuration to Achieve Output-Voltage Sharing for HV Generator Applications. *IEEE Trans. Power Electron.* **2019**, *34*, 6108–6122. [[CrossRef](#)]
32. Cheng, C.W.; Zhou, Z.; Li, W.G.; Zhu, C.; Deng, Z.F.; Mi, C.C. A Multi-Load Wireless Power Transfer System with Series-Parallel-Series Compensation. *IEEE Trans. Power Electron.* **2019**, *34*, 7126–7130. [[CrossRef](#)]
33. Tian, S.J.; Kong, J.M.; Fan, X.Y.; Han, P.F.; Sun, X.P. Series and parallel model of landslide hazard evaluation based on disaster conditions and application. *J. Natural Disasters* **2018**, *27*, 52–58.
34. Dlamini, W.M. A Bayesian belief network analysis of factors influencing wildfire occurrence in Swaziland. *Environ. Modell. Softw.* **2010**, *25*, 199–208. [[CrossRef](#)]
35. Sakai, C.; Iguchi, K.; Tachi, T.; Noguchi, Y.; Katsuno, S.; Teramachi, H. Factors Influencing Medicine Use Behavior in Adolescents in Japan Using a Bayesian Network Analysis. *Front. Pharmacol.* **2019**, *10*, 494. [[CrossRef](#)] [[PubMed](#)]
36. Lee, D.; Berberidis, D.; Giannakis, G.B. Adaptive Bayesian Radio Tomography. *IEEE Trans. Signal Process.* **2019**, *67*, 1964–1977. [[CrossRef](#)]
37. Vemulapalli, V.; Qu, J.Q.; Garren, J.M.; Rodrigues, L.O.; Kiebish, M.A.; Sarangarajan, R.; Narain, N.R.; Akmaev, V.R. Non-obvious correlations to disease management unraveled by Bayesian artificial intelligence analyses of CMS data. *Artif. Intell. Med.* **2016**, *74*, 1–8. [[CrossRef](#)]
38. Trifonova, N.; Karnauskas, M.; Kelble, C. Predicting ecosystem components in the Gulf of Mexico and their responses to climate variability with a dynamic Bayesian network model. *PLoS ONE* **2019**, *14*, e0209257. [[CrossRef](#)]
39. Fabbri, A.G.; Remondo, J.; Chung, C.J. Landslide Risk Assessment with Uncertainty of Hazard Class Membership. An Application of Favourability Modeling in the Deba Valley Area, Northern Spain. *Eng. Geol. Soc. Territ.* **2015**, *2*, 1759–1762. [[CrossRef](#)]
40. Chang-Jo, F.C.; Andrea, G.F. Validation of Spatial Prediction Models for Landslide Hazard Mapping. *Nat. Hazards* **2003**, *30*, 451–472. [[CrossRef](#)]
41. Pei, R.R.; Ni, Z.Q.; Meng, Z.B.; Zhang, B.L.; Geng, Y.Y. Cause Analysis of the Secondary Mountain Disaster Chain in Wenchuan Earthquake. *Am. J. Civil Eng.* **2017**, *5*, 414–417. [[CrossRef](#)]
42. Wang, M.; Liu, M.; Yang, S.N.; Shi, P.J. Incorporating Triggering and Environmental Factors in the Analysis of Earthquake-Induced Landslide Hazards. *Int. J. Disaster Risk Sci.* **2014**, *5*, 125–135. [[CrossRef](#)]
43. Hariklia, D.S.; George, D.B.; Efterpi, K.; Konstantinos, S.; Dimitrios, R. Physical and Anthropogenic Factors Related to Landslide Activity in the Northern Peloponnese, Greece. *Land* **2018**, *7*, 85. [[CrossRef](#)]
44. Li, X.; Liu, X.L.; Li, J.G.; Wang, Q.L.; Liao, W.L.; Zhang, L.F. Factor analysis of earthquake-induced geological disasters of the M7.0 Lushan earthquake in China. *Geod. Geodyn.* **2013**, *4*, 22–29. [[CrossRef](#)]
45. Wang, Y.; Fang, Z.C.; Hong, H.Y. Comparison of convolutional neural networks for landslide susceptibility mapping in Yanshan County, China. *Sci. Total Environ.* **2019**, *666*, 975–993. [[CrossRef](#)]

46. Lupiano, V.; Rago, V.; Terranova, O.G.; Iovine, G. Landslide inventory and main geomorphological features affecting slope stability in the Picentino river basin (Campania, southern Italy). *J. Maps* **2019**, *15*, 131–141. [[CrossRef](#)]
47. Tsangaratos, P.; Ilia, I.; Hong, H.Y.; Chen, W.; Xu, C. Applying Information Theory and GIS-based quantitative methods to produce landslide susceptibility maps in Nancheng County, China. *Landslides* **2017**, *14*, 1091–1111. [[CrossRef](#)]
48. Akgun, A. A comparison of landslide susceptibility maps produced by logistic regression, multi-criteria decision, and likelihood ratio methods: A case study at İzmir, Turkey. *Landslides* **2012**, *9*, 93–106. [[CrossRef](#)]
49. Ali, S.; Biermanns, P.; Haider, R.; Reicherter, K. Landslide susceptibility mapping by using a geographic information system (GIS) along the China-Pakistan Economic Corridor (Karakoram Highway), Pakistan. *Nat. Hazards Earth Syst. Sci.* **2019**, *19*, 999–1022. [[CrossRef](#)]
50. Shrestha, S.; Kang, T.S.; Choi, J.C. Assessment of co-seismic landslide susceptibility using LR and ANCOVA in Barpak region, Nepal. *J. Earth Syst. Sci.* **2018**, *127*, 38. [[CrossRef](#)]
51. Chen, J.J.; Cao, C.; Qin, S.W.; Peng, S.Y.; Ma, Q.; Liu, X.; Zhai, J.J. Debris flow susceptibility mapping using an improved information value model based on a combined weighting method for Jilin province, China. *Fresenius Environ. Bull.* **2018**, *27*, 9706–9716.
52. Kang, S.; Lee, S.R. Debris flow susceptibility assessment based on an empirical approach in the central region of South Korea. *Geomorphology* **2018**, *308*, 1–12. [[CrossRef](#)]
53. Cao, C.; Zheng, L.J.; Liu, Y.W.; Chen, D.H. An Approach to Assess Debris Flow Susceptibility. *Fresenius Environ. Bull.* **2018**, *27*, 7572–7578.
54. Charniak, E. Bayesian networks without tears. *AI Mag.* **1991**, *12*, 50–63. [[CrossRef](#)]
55. Masmoudi, K.; Abid, L.; Masmoudi, A. Credit risk modeling using Bayesian network with a latent variable. *Expert Syst. Appl.* **2019**, *127*, 157–166. [[CrossRef](#)]
56. Ghribi, A.; Masmoudi, A. A Compound Poisson Model for Learning Discrete Bayesian Networks. *Acta Math. Sci.* **2013**, *33*, 1767–1784. [[CrossRef](#)]
57. Castelletti, A.; Soncini-Sessa, R. Bayesian Networks and participatory modeling in water resource management. *Environ. Modell. Softw.* **2007**, *22*, 1075–1088. [[CrossRef](#)]
58. Joseph, S.A.; Adams, B.J.; McCabe, B. Methodology for Bayesian Belief Network Development to Facilitate Compliance with Water Quality Regulations. *J. Infrastruct. Syst.* **2010**, *16*, 58–65. [[CrossRef](#)]
59. Nadkarni, S.; Shenoy, P.P. A Bayesian network approach to making inferences in causal maps. *Eur. J. Oper. Res.* **2001**, *128*, 479–498. [[CrossRef](#)]
60. Kabir, G.; Tesfamariam, S.; Francisque, A.; Sadiq, R. Evaluating risk of water mains failure using a Bayesian belief network model. *Eur. J. Oper. Res.* **2015**, *240*, 220–234. [[CrossRef](#)]
61. Wang, C. The Research of Seismic Influence Filed and Intensity Attenuation. Master's Thesis, Southwest JiaoTong University, Chengdu, China, 2014.
62. Shen, W.H.; Zhong, Q.; Shi, B.P. Synthetic seismic intensity for historic earthquakes in the North China Plain: Implications for the regional seismic hazard. *Nat. Hazards* **2014**, *74*, 305–323. [[CrossRef](#)]
63. Cui, X.; Miao, Q.J.; Wang, J.P. Model of the Seismic Intensity Attenuation for North China. *North China Earthq. Sci.* **2010**, *28*, 18–21. [[CrossRef](#)]
64. Tang, Z.; McCabe, B. Developing Complete Conditional Probability Tables from Fractional Data for Bayesian Belief Networks. *J. Comput. Civil. Eng.* **2007**, *21*, 265–276. [[CrossRef](#)]
65. Di Baldassarre, G.; Nohrstedt, D.; Mard, J.; Burchardt, S.; Albin, C. An Integrative Research Framework to Unravel the Interplay of Natural Hazards and Vulnerabilities. *Earth Future* **2018**, *6*, 305–310. [[CrossRef](#)]

66. Qiu, J.N.; Liu, L.L.; Dong, L.L. Modeling method and application of emergent event chain based on Bayesian network. *J. Syst. Eng.* **2012**, *27*, 739–750.
67. Hilvano, N.F.; Nelson, G.L.M.; Coladilla, J.O.; Rebancos, C.M. Household Disaster Resiliency on Typhoon Haiyan (Yolanda): The Case of Manicani Island, Guiuan, Eastern Samar, Philippines. *Coast Eng. J.* **2016**, *58*, 1640007. [[CrossRef](#)]
68. Vakhshoori, V.; Pourghasemi, H.R. A novel hybrid bivariate statistical method entitled FROC for landslide susceptibility assessment. *Environ. Earth Sci.* **2018**, *77*, 686. [[CrossRef](#)]
69. Fawcett, T. An introduction to ROC analysis. *Pattern Recognit. Lett.* **2006**, *27*, 861–874. [[CrossRef](#)]



© 2019 by the authors. Licensee MDPI, Basel, Switzerland. This article is an open access article distributed under the terms and conditions of the Creative Commons Attribution (CC BY) license (<http://creativecommons.org/licenses/by/4.0/>).